PHYSICAL REVIEW B VOLUME 18, NUMBER 4 15 AUGUST 1978

Molecular dynamics of shock waves in one-dimensional chains

B. L. Holian and G. K. Straub
Los Alamos Scientific Laboratory, Los Alamos, New Mexico 87544
(Received 30 January 1978)

The behavior of shock waves in one-dimensional chains has been explored in a series of molecular-dynamics computer experiments. Three "realistic" nearest-neighbor pair potentials were considered—Lennard-Jones 6-12, Toda, and Morse—as well as three truncated forms—harmonic, cubic, and quartic. Over a wide range of shock strengths the particle velocity profiles and shock speeds for a given form of potential can be characterized in strength by αv, where α is the cubic anharmonicity coefficient and v is the particle velocity in units of the long-wavelength sound speed. For strong shocks ($\alpha v > 1$), steady hard-rod-like velocity profiles are observed for the "realistic" potentials and the quartic truncated form, but not for the harmonic or cubic forms. The shock thickness in the harmonic chain grows as the cube root of time, while the shock thickness in the anharmonic chain grows linearly with time, in proportion to shock strength. This evolution of the shock thickness is unaffected by initial equilibration of the chain at finite temperature. If either a heavy- or light-mass defect is included, the shock wave is reflected and the relaxation process is slowed behind the defect.

I. INTRODUCTION

There have been several previous molecular-dynamics studies of the nature of shock waves in one, two, and three dimensions.[1-8] The motivation for the current work is to understand the various mechanisms that determine the width of a shock wave in a solid and the final state of the material behind the shock front.

In our view, a shock wave propagating through a solid consists of three highly coupled processes: initial elastic response, thermal equilibration, and plastic stress relaxation. First, the initial elastic excitation of the material by a wave front propagating at the shock velocity can be characterized by a rise time, which for a shock velocity on the order of 10 km/sec in a material with a lattice spacing of 1 Å is about 10^{-14} sec. The results of our calculations give rise times in rough agreement with this estimate. Following the initial rise, thermodynamic quantities will overshoot what will be their final equilibrium values. The second and third processes, which can occur simultaneously, are an approach to equilibrium of all thermodynamic quantities coupled with the relaxation of internal stresses usually associated with plastic flow. Internal stress relaxation begins immediately after the shock front passes but can persist long after thermodynamic equilibrium is attained.

We wish to emphasize the difference in time scales for the two processes. For small local thermal fluctuations, thermodynamic equilibrium can be reached in about 10^{-13} sec, a typical vibrational period in a solid. Most continuum hydrodynamic calculations of shock waves assume thermodynamic equilibrium at all times for plastic flow on a time scale of 10^{-9}–10^{-6} sec and achieve good agreement with experimentally measured wave profiles. Anisotropic stress distribution can persist long after thermodynamic equilibrium is established behind the shock front.[9] The purpose of this paper is to explore the regime where thermodynamic equilibrium has not been obtained, so that the assumptions of continuum mechanics[10] must be questioned.

For one-dimensional systems shear stress relaxation cannot occur and hence must be studied in three dimensions. We have focused our attention on how thermodynamic equilibrium is attained following excitation by a shock wave on a lattice of discrete particles in one dimension; that is, we want to know how the local dynamical variables such as density, particle velocity, and temperature relax to their new values behind the shock front. Three "realistic" nearest-neighbor potentials were considered: Lennard-Jones 6-12, Toda, and Morse. While the Lennard-Jones potential has fixed anharmonicity, the anharmonicity of the Morse and Toda potentials can be continuously varied. The Toda potential is particularly interesting because it can be varied from the harmonic limit to the hard-sphere limit. In addition, we have studied three truncated forms: the harmonic, the harmonic plus cubic, and the harmonic plus cubic and quartic. Over a wide range of shock strengths the particle velocity profiles and shock speeds for a given form of potential can be characterized by αv, where α is the cubic anharmonicity coefficient and v is the particle velocity in units of the long-wavelenth sound speed.

In Sec. II we give a brief outline of the molecular-dynamics method using the central difference

 © 1978 The American Physical Society

approximation. Section III contains details of the pair potentials that were used. In Sec. IV we give a review of shock-wave propagation in the hard-rod chain. Besides illustrating many of the general features of shock waves, we find that the strong shock ($\alpha v > 1$) behavior of all but the harmonic and cubic potentials qualitatively approach that of the hard-rod chain. We have also calculated the effect of a mass defect in the hard-rod system and find that the shock structure is altered for either a lighter or heavier particle, with energy scattered backward down the chain.

The analytic solutions to the harmonic chain outlined by Manvi *et al.*[2] are discussed in Sec. V and compared with our molecular-dynamics results. We have also calculated the relaxation time of the particle velocity (which gives the shock width in the absence of stress relaxation) and find that the shock width grows with time t as $t^{1/3}$. (The same qualitative results apply for the relaxation of density, stress, and temperature.) For the other anharmonic potentials we determine in Sec. VI a relaxation time that grows as t. The $t^{1/3}$ growth of the relaxation time in the harmonic system conforms to the accepted continuum description of shock waves where the shock thickness of unequilibrated material is small compared to the extent of equilibrated material on both sides of the shock front. The linear growth of the shock thickness with time observed in the anharmonic systems does not conform to the usual continuum notions, since the unequilibrated region is a constant fraction of the material behind the shock front. Calculations we have done in three dimensions at finite temperature for anharmonic potentials also predict that the shock thickness will grow linearly in time. We find no relation, in any of the one- or three-dimensional calculations we have done, between the shock width and the propagation velocity of second sound as previously reported by Tsai and MacDonald.[8]

In Sec. VII the effects of finite initial temperatures and mass defects for continuous potentials are presented. A finite initial temperature seems to have no observable effect on the approach to equilibrium. We observe a change in temperature only following a sufficiently strong shock. We do find behavior qualitatively similar to the hard-rod chain for mass defects. In general, the interaction of a shock wave with a mass defect scatters the wave, so that the time required to reach thermodynamic equilibrium is lengthened.

Our numerical calculation of a very weak shock in the harmonic plus cubic truncated potential does not agree with the far-field perturbative solution of Tasi.[7] We do not see the same qualitative behavior in the particle-velocity profiles that Tasi identifies as solitary waves. We do see steady wave profiles qualitatively similar to the hard-rod system for strong shocks ($\alpha v > 1$) in chains where the potential has at least some quartic anharmonicity.

II. MOLECULAR-DYNAMICS METHOD

The method of integrating on the computer the classical equations of motion for a large number of interacting particles is known as molecular dynamics.[11-13] We will briefly outline the method as it applies to one-dimensional chains. The position of particle N at time t is given by $X_N(t)$. The displacement of particle N from its original position is

$$x_N(t) = X_N(t) - X_N(0) . \tag{1}$$

Initially, the particles $N = 0, 1, 2, 3, \ldots$, are placed at lattice sites $X_N(0) = Na$, where a is the lattice spacing. The relative displacement of particles i and j is given by

$$x_{ij} = x_i - x_j . \tag{2}$$

The equations of motion for continuous nearest-neighbor interactions in the one-dimensional chain are given by

$$m \frac{d^2 X_N(t)}{dt^2} = F_N(t) = F_{N,N-1}(t) + F_{N,N+1}(t) , \tag{3}$$

where m is the mass of the particle, F_N is the force on particle N, and F_{ij} is the force on particle i due to particle j. For particles interacting via a central, pairwise-additive potential ϕ, we have

$$\begin{aligned} F_{ij}(t) &= -\phi'(|X_i(t) - X_j(t)|) \\ &= -F_{ji}(t) . \end{aligned} \tag{4}$$

The last line expresses the law of equal but opposite interactions between pairs of particles. We shall use primes to indicate spatial derivatives and dots for time derivatives. The equations of motion can be rewritten in terms of displacements:

$$m\ddot{x}_N(t) = F_N(t) = \phi'(a + x_{N+1,N}) - \phi'(a + x_{N,N-1}) . \tag{5}$$

In order to integrate Eq. (5), a finite time step Δt is introduced and the trajectory of each particle is discretized. The change in displacement x_N during the time interval from t to $t + \Delta t$ is

$$\Delta x_N(t + \Delta t) = \Delta x_N(t) + F_N(t)(\Delta t)^2/m . \tag{6}$$

The displacement x_N is then advanced each time step:

$$x_N(t + \Delta t) = x_N(t) + \Delta x_N(t + \Delta t) , \tag{7}$$

with velocities given by

$$\dot{x}_N(t+\Delta t)=\Delta x_N(t+\Delta t)/\Delta t\,. \tag{8}$$

The last three equations constitute the straightforward central-difference approximation to Eq. (5) (strictly speaking, for changes in displacements and for velocities, the time arguments shown here as $t+\Delta t$ are really at $t+\frac{1}{2}\Delta t$). To begin the calculation, one needs to specify initial positions (lattice sites) and velocities of the particles as well as any additional boundary conditions that represent external forces.

In order to simplify notation we let the unit of length be a, the lattice spacing, and the unit of time be $1/\omega_0$, where ω_0 is the fundamental harmonic frequency given by $m\omega_0^2=\phi''(a)$. If ϕ' is expanded in a Taylor series about the equilibrium lattice spacing a for small relative displacements x_{ij},

$$\phi'(a+x_{ij})=\phi'(a)+\phi''(a)x_{ij}+\tfrac{1}{2}\phi'''(a)x_{ij}^2 +\tfrac{1}{6}\phi''''(a)x_{ij}^3+\cdots\,, \tag{9}$$

and the new time and distance units introduced, then the equations of motion, Eq. (5), can be rewritten

$$\ddot{x}_N(t)=x_{N+1,N}-x_{N,N-1}-\alpha(x_{N+1,N}^2-x_{N,N-1}^2 +\beta(x_{N+1,N}^3-x_{N,N-1}^3)+\cdots\,, \tag{10}$$

where α is the cubic anharmonicity coefficient,

$$\alpha=-\tfrac{1}{2}a\phi'''(a)/\phi''(a)\,, \tag{11}$$

and β is the quartic anharmonicity coefficient,

$$\beta=\tfrac{1}{6}a^2\phi''''(a)/\phi''(a)\,. \tag{12}$$

(For most realistic potentials, α is on the order of 10, while β is on the order of 100.) With these new time and distance units, the velocity unit is

$$c_0=a\omega_0\,, \tag{13}$$

the long-wavelength sound speed in the harmonic chain ($\alpha=\beta=\cdots=0$). The particle velocity u_p and the shock velocity u_s in the new units are then

$$v=u_p/c_0\,;\quad \mu=u_s/c_0\,. \tag{14}$$

The zero-temperature initial conditions for $N\geq 1$ are

$$x_N(0)=0\,;\quad \dot{x}_N(0)=0\,;\quad \ddot{x}_N(0)=0\,. \tag{15}$$

To initiate a shock wave, we consider the first particle on the chain $[N=0, X_0(0)=0]$ to be infinitely massive, in essence, the "piston," with constant velocity

$$\dot{x}_0(t)=v\,, \tag{16}$$

for $t\geq 0$.

The time step Δt was chosen such that $\omega_0\Delta t=0.1$ for shock strength $\alpha v\leq 0.525$. (In a later section, the characterization of shock strength by the product αv is discussed. Multiples of $\alpha=10.5$, the Lennard-Jones 6-12 pair potential cubic anharmonicity coefficient, appear frequently in our calculations; for example, a relatively weak shock with $\alpha=10.5$ and $v=0.05$ has a shock strength of $\alpha v=0.525$.) This choice makes the time step about $\frac{1}{30}$th of the period of the maximum frequency of the harmonic chain, $2\omega_0$. For larger values of αv the time step was scaled downward: $\omega_0\Delta t=0.0525/\alpha v$. Variations in Δt by a factor of 2, either larger or smaller, produced no noticeable change in the calculated solutions.

III. PAIR POTENTIALS

In this study of one-dimensional shock waves, several different forms of pair potentials with varying degrees of anharmonicity have been used. These include the Lennard-Jones (LJ) 6-12 potential [presented in reduced units so that $\phi''(1)=1$ and $\phi(1)=\phi'(1)=0$]:

$$\phi(x)=\tfrac{1}{72}(x^{-12}-2x^{-6}+1)\,, \tag{17}$$

where $\alpha=10.5$ and $\beta=\frac{106}{189}\alpha^2=0.560\,847\alpha^2$; the Toda potential[14]:

$$\phi(x)=(1/4\alpha^2)\{\exp[-2\alpha(x-1)] +2\alpha(x-1)-1\}\,, \tag{18}$$

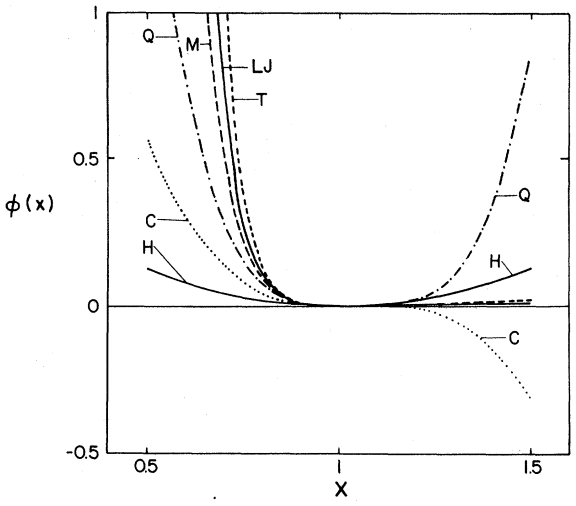

FIG. 1. Pairwise-additive potential $\phi(x)$ as a function of particle separation x. H—harmonic ($\alpha=\beta=0$), C—cubic ($\alpha=10.5$, $\beta=0$), and Q—quartic ($\alpha=10.5$, $\beta=73.5$) are truncated potentials: $\phi(x)=\frac{1}{2}(x-1)^2-\frac{1}{3}\alpha(x-1)^3+\frac{1}{4}\beta(x-1)^4$. LJ is Lennard-Jones 6-12 potential defined in Eq. (17); T is Toda potential ($\alpha=10.5$) defined in Eq. (18); and M is Morse potential ($\alpha=10.5$) defined in Eq. (19).

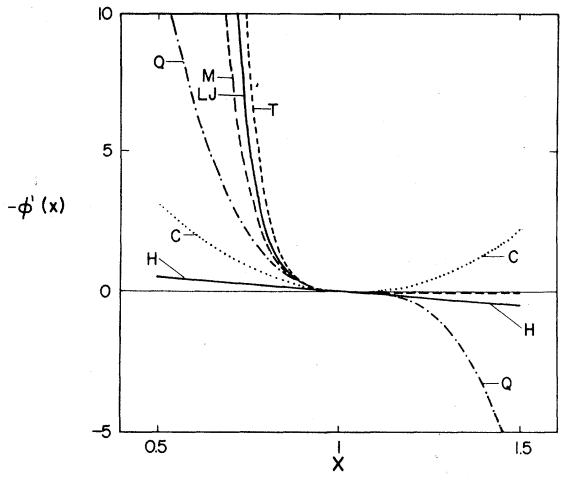

FIG. 2. Pairwise-additive force $-\phi'(x)$ as a function of particle separation x. (Same key as Fig. 1.)

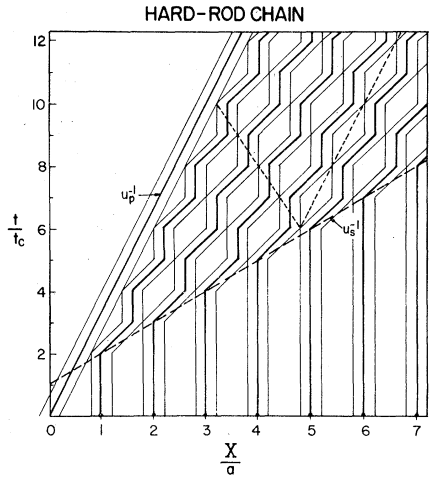

FIG. 3. Shock-wave trajectories of hard rods in a one-dimensional chain: positions X/a as a function of time t/t_c (a is lattice spacing, t_c is collision time). The hard-rod length σ is $\frac{2}{5}a$. The shock velocity (long dashes) is $u_s = a/t_c$, while the particle velocity (straight line) for the piston rod, which starts out at $X=0$ at $t=0$, is $u_p = 0.3\,u_s$. The lines emanating from the point of contact of particles 4 and 5 (short dashes) are shown for reference to Fig. 6.

where α can be varied from zero, the harmonic limit, to infinity, the hard rod limit (that is, hard spheres in one dimension), and $\beta = \frac{2}{3}\alpha^2$; and the Morse potential:

$$\phi(x) = (9/8\alpha^2)\{\exp[-\tfrac{4}{3}\alpha(x-1)] - 2\exp[-\tfrac{2}{3}\alpha(x-1)] + 1\}, \quad (19)$$

where $\beta = \frac{14}{27}\alpha^2 = 0.518\,518\cdots\alpha^2$. In addition to these "realistic" potentials, three truncated forms were considered: harmonic ($\alpha=\beta=0$), cubic ($\beta=0$), and quartic. The potentials ϕ are shown in Fig. 1 and the forces $-\phi'$ in Fig. 2 as functions of the interatomic separation. The Toda and Morse potentials shown have $\alpha = 10.5$, the LJ 6-12 value. However, since the values of β differ, the stiffness of the repulsive wall is in the order Toda > LJ 6-12 > Morse (β/α^2: 0.667 > 0.561 > 0.519). The harmonic, cubic, and quartic potentials are truncated forms of the Toda $\alpha = 10.5$ potential.

IV. HARD-ROD CHAIN

It is instructive to review shock-wave propagation in the hard-rod chain, since the analysis is simple and serves to illustrate many of the features of the problem for more realistic interactions. Hard rods, the one-dimensional analog of three-dimensional hard spheres, interact only on contact with one another via perfectly elastic collisions. The natural unit of time in the zero-temperature hard-rod shock-wave problem is the collision time given by

$$t_c = (a-\sigma)/2u_p, \quad (20)$$

where σ is the length of the hard rods. In Fig. 3 the trajectories of the hard rods are shown as they evolve with time. At time $2t_c$ the "piston" rod ($N=0$), which always travels at velocity u_p, hits the first rod ($N=1$) which then begins traveling toward the second ($N=2$) at velocity $2u_p$. At $3t_c$, $N=1$ hits $N=2$ and comes to rest while $N=2$ moves off at velocity $2u_p$. The collision chain proceeds at intervals of t_c so that the shock front moves out ahead of the piston at the shock velocity

$$u_s = a/t_c = 2u_p/(1-\sigma/a), \quad (21)$$

indicated by the dashed line in Fig. 3. The $N=1$ rod is again struck from behind by the piston, and henceforth, follows an oscillatory trajectory between its two nearest neighbors. In Fig. 4, the steady square-wave velocity profile, characteristic of a shock wave in a hard-rod system, is shown for a given particle along with its displacement as a function of time. There is no dispersion in the velocity-profile since there is but one frequency, namely, $2\pi/t_c$.

This information of Figs. 3 and 4 is displayed in Fig. 5 as a contour plot of velocity versus position and time (only one contour, at $2u_p$, has been drawn). Note the series of peaks paralleling the shock front as well as ones more or less perpendicular to the front. These peaks and troughs arise from the discrete nature of the lattice and appear also in shock-wave propagation in chains of particles interacting via more realistic potentials.

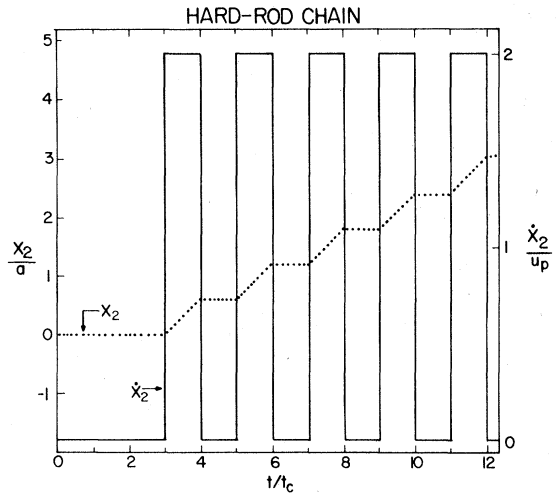

FIG. 4. Velocity response $\dot{x}_2$ (straight line) of hard-rod number two to the shock wave as a function of time; its displacement x_2 from its lattice site $X_2(0)=2a$ is also shown (dots).

From Eq. (21), we note that the relative compression behind the shock,

$$\eta = 1/(1-u_p/u_s) = 2/(1+\sigma/a)\,, \tag{22}$$

is independent of the particle velocity and depends only on the relative excluded volume per particle, σ/a. As the relative free volume per particle $(1-\sigma/a)$ decreases, the proportionality between the shock and particle velocities increases, much as stiffening the repulsive wall of realistic potentials by increasing the anharmonicity α will be shown to increase the slope of u_s vs u_p.

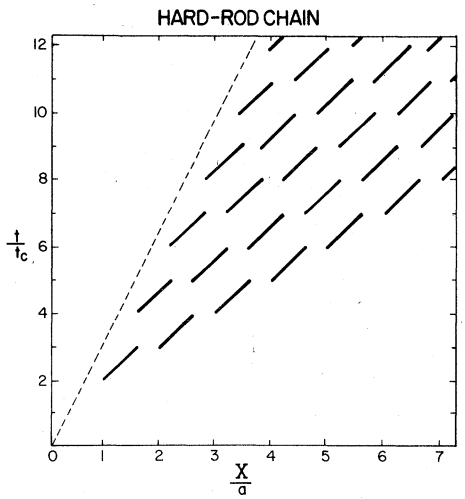

FIG. 5. Velocity contour plot for a shock wave in a one-dimensional chain of hard rods as a function of position and time (see Fig. 3). A contour is drawn at velocity $2u_p$. The dashed line shows the trajectory of the piston particle.

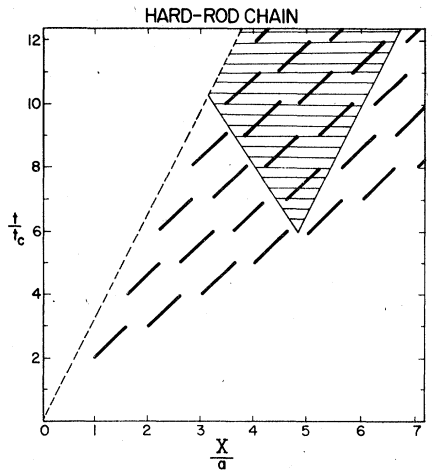

FIG. 6. Velocity contour plot for a shock wave in a one-dimensional chain of hard rods with the fifth rod having a slightly different mass from the rest of the rods: $m_5/m = 1+\delta$, $|\delta| \ll 1$. The shaded area is the region of backscattered interference from the mass defect. The inverse of the slope of the left-most boundary of the shaded region is V_r, the reflection velocity [Eq. (23)]. Compare with Fig. 3.

The effect of a slight mass defect can be seen in Fig. 6, where $N=5$ is the defective rod carrying a massless Maxwell demon determined to ride the rods, as though they were boxcars, from $N=5$ to $N=0$, the piston. Imagine further that the demon can only jump from one "boxcar" to the next at the moment they collide. Therefore, his path will be somewhere in the shaded region, depending on his bravery and timing (see also in Fig. 3 the region between the dotted lines). If he is quick and brave, he will follow the left-hand line toward the piston at the reflection velocity V_r (with respect to the already shocked boxcars moving at an average velocity u_p). If, on the other hand, he is too slow or scared, he will ride the fifth boxcar at an average velocity of u_p along the right-hand border of the shaded region.

Now consider the case of a real mass defect at $N=5$, namely, the mass is $m(1+\delta)$, where $-1<\delta<\infty$ (m is the mass of all the other particles, except the infinitely massive piston). The reflection velocity due to the mass defect is found to be

$$V_r = -(u_s/\eta)[1+\tfrac{1}{2}\delta(1+\eta)]/(1+\tfrac{1}{2}\delta)\,. \tag{23}$$

The new shock velocity ahead of the defect will then be

$$u_s' = u_s(1+\delta)/(1+\tfrac{1}{2}\delta)^2\,, \tag{24}$$

which is slower than u_s to second order in δ. The

average velocity of the defect particle is similarly slower than the average particle velocity to second order in δ. Thus, whether the defect is light or heavy, energy is scattered back toward the piston, affecting the dynamical history in the shaded region in Fig. 6. (These results will be compared to the behavior of chains with more realistic interactions in Sec. VII.)

V. HARMONIC CHAIN

At the other extreme of interaction is the harmonic chain, where particles interact with their nearest neighbors through a force linear in relative displacement. To further illustrate the framework for the general case to be presented in following sections, the analytical solution for shock waves in the harmonic chain will now be briefly outlined. The equations of motion [Eq. (10)] are given by

$$\ddot{x}_N(t) = x_{N-1}(t) - 2x_N(t) + x_{N+1}(t) . \tag{25}$$

The analytical solution satisfying the shock boundary conditions, Eqs. (15) and (16), has been shown[2] to be a series of Bessel functions of the first kind for particle displacements

$$x_N(t) = \nu \sum_{k=0}^{\infty} (2k+1) J_{2k+1}(2t) , \tag{26}$$

with particle velocities given by

$$\dot{x}_N(t) = \frac{\nu}{t} \sum_{k=N}^{\infty} (2k+1) J_{2k+1}(2t)$$

$$= \nu \left[1 + J_0(2t) + J_{2N}(2t) - 2 \sum_{k=0}^{N} J_{2k}(2t) \right] , \tag{27}$$

and particle accelerations given by

$$\ddot{x}_N(t) = (2\nu N/t) J_{2N}(2t) . \tag{28}$$

The final state of the chain behind the shock front is $\dot{x}_N \to \nu$ and $\ddot{x}_N \to 0$. The shock velocity is $\mu \sim 1$, since particle N begins to move only when $t \sim N$ [$J_n(z)$ is small until $z \sim n$], regardless of ν. In order that particles not be sent through one another, however, ν must be less than μ.

The most useful diagnostic in the shock-wave problem is the velocity profile $\dot{x}_N(t)/u_p$. For the harmonic chain, the analytic expression for the velocity profile, Eq. (27), is unfortunately very difficult to compute, since the important features for particles far from the piston ($N \gtrsim 100$) are given by high-order Bessel functions where the arguments are close to the orders. We can, however, compare the times for the first and second peaks in the velocity profile of particle N, $t_N^{(1)}$, and $t_N^{(3)}$, respectively ($t_N^{(2)}$ is for the first trough), as given by the molecular-dynamics experiment and by the first and third zeros of the asymptotic analytic expression [Eq. (28)][15]:

$$t_N^{(j)} = N + \tfrac{1}{2}(-a_j) N^{1/3} , \tag{29}$$

where $j = 1, 2, 3, \ldots$, and a_j are the negative zeros of the Airy function $\mathrm{Ai}(x)$. For $N = 751$, we observe $t_{751}^{(1)} = 761.6$ and calculate from Eq. (29) 761.6; $t_{751}^{(3)} = 776.2$ is observed while 776.1 is calculated, well within the $O(1/N)$ accuracy of Eq. (29). We conclude that even after long times, namely, more than 7500 time steps, the numerical integration of the equations of motion is very accurate.

From Eq. (29) for $j = 1$ and particles N, $N+1 \gg 1$ we find that

$$\mu = 1 - \tfrac{1}{6}(-a_1) N^{-2/3} + \cdots . \tag{30}$$

The initial oscillatory period of particle N is given by

$$t_N^{(1,3)} = t_N^{(3)} - t_N^{(1)} = \tfrac{1}{2}(-a_3 + a_1) N^{1/3} , \tag{31}$$

whence the initial oscillatory frequency is

$$\omega_1(N) = 2\pi / t_N^{(1,3)} = [4\pi/(-a_3 + a_1)] N^{-1/3} . \tag{32}$$

Since the dispersion relation for the harmonic chain yields the following frequency dependence for wave velocity[16]

$$c(\omega) = c_0 (1 - \omega^2/4\omega_0^2)^{1/2} , \tag{33}$$

we are led to compare the shock velocity as a function of particle number [Eq. (30)] with

$$c(\omega_1) = 1 - [2\pi^2/(-a_3 + a_1)^2] N^{-2/3} + \cdots . \tag{34}$$

(The coefficient multiplying $N^{-2/3}$ is about five times larger in the latter expression than in the former, though they are in basic agreement.)

The velocity profiles of several particles in the harmonic chain are presented in Fig. 7(a), with abbreviated profiles, that is, initial rises and peak positions, presented in Fig. 7(b). The initial peak response to the propagating shock-wave asymptotes to $1.27u_p$ by about particle number 50. The initial rise becomes less steep with particle number, though the arrival time $t_N^{(0)} = N$ correlates well with an approximately constant velocity, $\sim 0.36u_p$. [It may not be completely coincidental that $\mathrm{Ai}(0) = 0.355$.] The initial period of oscillation steadily increases with particle number, hence $\mu \to 1$ (the fastest propagation speed in a harmonic chain is for low-frequency waves: c_0). The long-time value of the oscillation period is π, corresponding to the highest frequency in the spectrum of the harmonic chain, $2\omega_0$. The velocity profiles oscillate about and decay to the particle velocity with time—exponentially at first and more slowly, $\sim t^{-1/2}$, at long times. The $1/e$-fold decay time $\tau_N^{1/e}$, defined as the largest value such that

$$\dot{x}_N(t_N^{(1)} + \tau_N^{1/e}) - u_p = [\dot{x}_N(t_N^{(1)}) - u_p]/e , \tag{35}$$

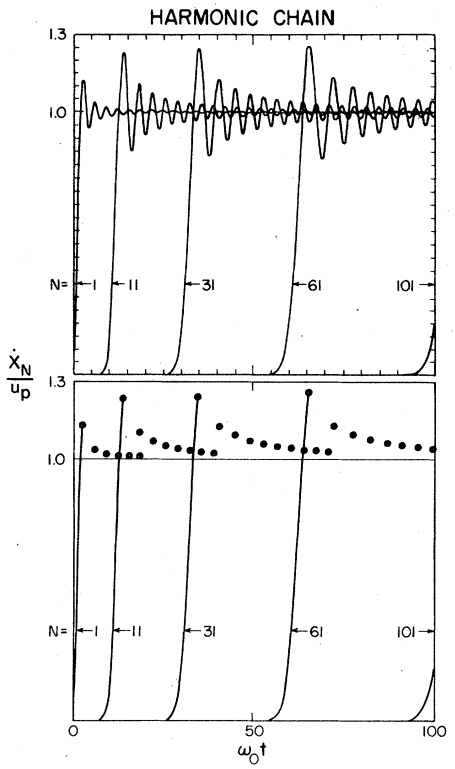

FIG. 7. Velocity profiles $\dot{x}_N/u_p$ vs time for several particles N in the harmonic chain. (a) Shows complete profiles, while (b) shows abbreviated profiles, i.e., the initial rise shown as a solid line and velocity peaks as dots.

increases with particle number in proportion to $N^{1/3}$. As shown in Fig. 8(a) and Table I, a similar result is obtained by fitting the first and second peaks to an exponential decay:

$$\tau_N^{\exp}=t_N^{(1,3)}/\ln\{[\dot{x}_N(t_N^{(1)})-u_p]/[\dot{x}_N(t_N^{(3)})-u_p]\}. \quad (36)$$

The ratio $\tau_N^{1/e}/\tau_N^{\exp}$ is essentially constant with N, about 1.06. Since we observe that $\dot{x}_N(t_N^{(1)})/u_p \to 1.272$ and $\dot{x}_N(t_N^{(3)})/u_p \to 1.152$, while from Eq. (31), $t_N^{(1,3)} \to 1.59N^{1/3}$; hence $\tau_N^{\exp} \to 2.73N^{1/3}$ and $\tau_N^{1/e} \to 2.90N^{1/3}$. If time is measured from the arrival time ($t_N^{(0)}=N$) through the region of $1/e$-fold decay ($t_N^{(0)}+\tau_N$) and divided by $N^{1/3}$, then for this time interval velocity profiles of different particles can be superimposed. The relaxation rear velocity u_r behind the shock front is given by

$$\frac{u_r}{u_s}=\frac{1+(u_p/u_s)(\tau_N/t_N^{(0)})}{1+\tau_N/t_N^{(0)}}, \quad (37)$$

so that $u_p<u_r<u_s$; observed and calculated (using the asymptotic behavior $\tau_N=2.90N^{1/3}$) values are given in Table I and Fig. 8(b). If, as in the hard-rod chain, relaxation is never achieved, then $u_r=u_p$. If τ_N is proportional to N, then u_r is a constant fraction of u_s of all times. On the other hand, if τ_N is proportional to N to some fractional power, like $\frac{1}{3}$ in the harmonic case, then $u_r \to u_s$. This conforms to the accepted continuum description of shock waves where the shock thickness of unequilibrated material is small compared to the

TABLE I. Arrival times, relaxation times, and relaxation rear velocity for the harmonic chain as functions of particle number N.

N	$t_N^{(1)}$	$\dot{x}_N^{(1)}/v$	$t_N^{(3)}$	$\dot{x}_N^{(3)}/v$	$t_N^{(1,3)}$	$t_N^{(1,3)}/N^{1/3}$	$\tau_N^{\exp}$	$\tau_N^{\exp}/N^{1/3}$	$t_N^{1/e}$	$\tau_N^{1/e}$	$\tau_N^{1/e}/\tau_N^{\exp}$	u_r/u_s obs	u_r/u_s calc
	(a)	(b)	(c)	(c)	(d)		(e)		(f)	(f)		(g)	(h)
31	34.6	1.251	40.4	1.130	5.8	1.85	8.8	2.81	40.9	6.3	0.72	0.854	0.784
61	65.8	1.259	72.4	1.139	6.6	1.68	10.6	2.69	77.8	12.0	1.13	0.853	0.850
101	106.2	1.261	114.2	1.143	8.0	1.72	13.3	2.86	120.6	14.4	1.08	0.887	0.888
151	157.2	1.267	166.0	1.146	8.8	1.65	14.6	2.74	173.4	16.2	1.11	0.911	0.912
211	217.8	1.267	227.8	1.147	10.0	1.68	16.8	2.81	235.6	17.8	1.06	0.928	0.928
281	288.6	1.269	299.4	1.149	10.8	1.65	18.3	2.79	308.1	19.5	1.07	0.940	0.940
361	369.4	1.270	380.8	1.150	11.4	1.60	19.4	2.72	390.3	20.9	1.08	0.949	0.949
451	459.8	1.270	472.4	1.151	12.6	1.64	21.7	2.83	482.5	22.7	1.05	0.955	0.955
551	560.6	1.271	573.8	1.151	13.2	1.61	22.6	2.75	584.6	24.0	1.06	0.961	0.961
751	761.6	1.272	766.2	1.152	14.6	1.61	25.1	2.76	788.3	26.7	1.06	0.968	0.968
∞						1.59		2.735					1.0

[a] $t_N^{(1)}$: arrival time for first peak in velocity.
[b] $\dot{x}_N^{(1)}$: first peak of velocity profile; v: reduced particle velocity, u_p/c_0.
[c] $t_N^{(3)}, \dot{x}_N^{(3)}$: second-peak quantities.
[d] $t_N^{(1,3)}=t_N^{(3)}-t_N^{(1)}$: initial oscillatory period [Eq. (31)].
[e] $\tau_N^{\exp}$: exponential-fit relaxation time [Eq. (36)].
[f] $t_N^{1/e}=t_N^{(1)}+\tau_N^{1/e}$; $\tau_N^{1/e}$: $1/e$-fold decay time [Eq. (35)].
[g] u_r: relaxation rear velocity [Eq. (37)]; u_s: shock velocity.
[h] Calculated using $u_p=0.05$, $u_s=1$, $t_N^{(0)}=N$, and $\tau_N=2.90N^{1/3}$.

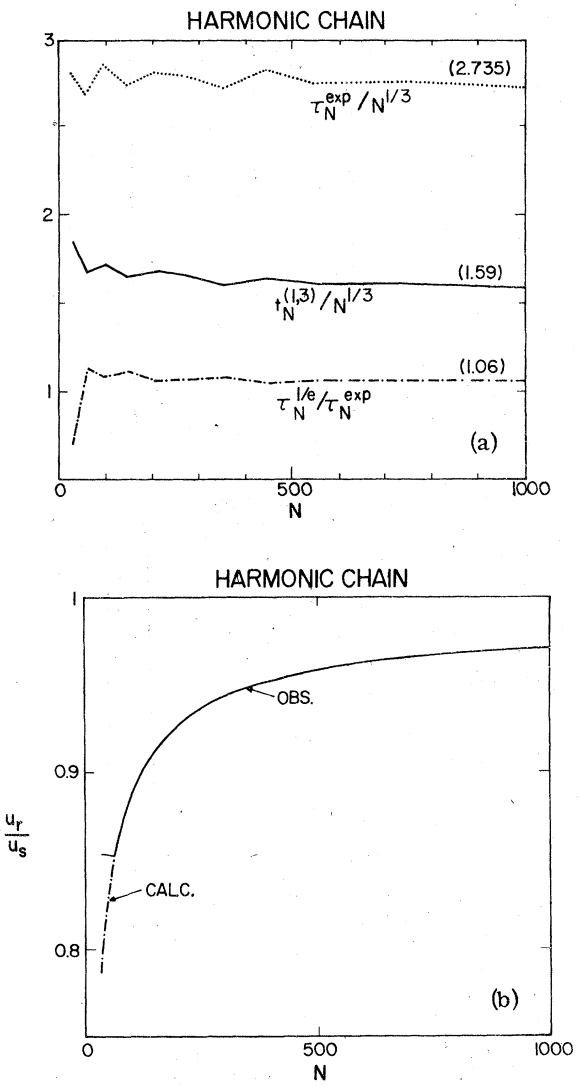

FIG. 8. Asymptotic behavior with distance into the harmonic chain, N: (a) exponential-fit relaxation time τ_N^{exp} [see Eq. (36)]; initial oscillatory period $t_N^{(1,3)}$ [see Eq. (31)]; and the ratio of the measured $1/e$-fold relaxation time $\tau_N^{1/e}$ to τ_N^{exp}; (b) observed and calculated ratios of the relaxation rear velocity u_r to the shock front velocity u_s. (See Table I.)

extent of equilibrated material on both sides of the shock front.

VI. MORE REALISTIC POTENTIALS

When varying degrees of anharmonicity are included in the interactions of particles in the one-dimensional chain, many of the features of the velocity profiles for weak shocks qualitatively resemble those exhibited by the harmonic chain. Comparison of Fig. 9(a) (Toda chain, $\alpha = 10.5$, $\nu = 0.05$) with Fig. 7(b) (harmonic chain, $\alpha = \beta = 0$, $\nu = 0.05$) shows that, for the anharmonic chain, the initial peak rises as a function of particle number and asymptotes to a higher value than in the harmonic chain, nearer to $2u_p$.[17] On the other hand, unlike the harmonic chain, the initial rise of a particle's velocity response does not noticeably broaden with distance into the chain from the piston particle. The initial oscillatory frequency ω_1 decreases to a limiting value with distance into the anharmonic chain, rather than approaching zero ($\sim N^{-1/3}$) as in the harmonic chain [see Eq. (32)]. The relaxation time τ_N grows linearly with particle number, which is much faster than the $N^{1/3}$ growth observed for the harmonic case. Consequently, the shock thickness is a constant fraction of the material behind the shock front, rather than a diminishing fraction with time as in the harmonic chain. This linear growth of shock thickness obviously does not agree with the concepts used to justify the usual continuum treatment of shock waves.

The shock velocity, for the same particle velocity, is greater in the anharmonic chain. The ve-

TABLE II. Shock velocity $\mu = u_s/c_0$ as a function of cubic anharmonicity α, quartic anharmonicity β, and particle velocity $\nu = u_p/c_0$ for a variety of nearest-neighbor interactions.

α	β/α^2	ν	$\alpha\nu$	μ	Comments
0.0	0.0	0.05	0.0	1.0	harmonic
10.5	0.0	0.01	0.105	1.061	cubic
10.5	0.667	0.01	0.105	1.066	Toda
10.5	0.0	0.05	0.525	1.25	cubic
10.5	0.519	0.05	0.525	1.30	Morse
10.5	0.561	0.05	0.525	1.31	LJ 6-12
10.5	0.667	0.05	0.525	1.30	quartic
10.5	0.667	0.05	0.525	1.33	Toda
1.05	0.667	0.5	0.525	1.33	Toda
10.5	0.0	0.1	1.05	1.40	cubic
10.5	0.667	0.1	1.05	1.63	Toda
10.5	0.667	0.15	1.575	1.90	Toda
10.5	0.667	0.18	1.89	2.08	Toda
10.5	0.0	0.2	2.1	1.64	cubic
10.5	0.667	0.2	2.1	2.19	Toda
10.5	0.0	0.5	5.25	2.05	cubic
10.5	0.519	0.5	5.25	3.19	Morse
10.5	0.561	0.5	5.25	3.37	LJ 6-12
10.5	0.667	0.5	5.25	2.86	quartic
10.5	0.667	0.5	5.25	3.61	Toda
105.0	0.667	0.05	5.25	3.61	Toda
10.5	0.0	1.0	10.5	2.60	cubic
10.5	0.667	1.0	10.5	5.79	Toda
10.5	0.667	2.0	21.0	5.00	quartic
10.5	0.667	2.0	21.0	9.61	Toda
10.5	0.667	5.0	52.5	19.7	Toda
105.0	0.667	0.5	52.5	19.7	Toda

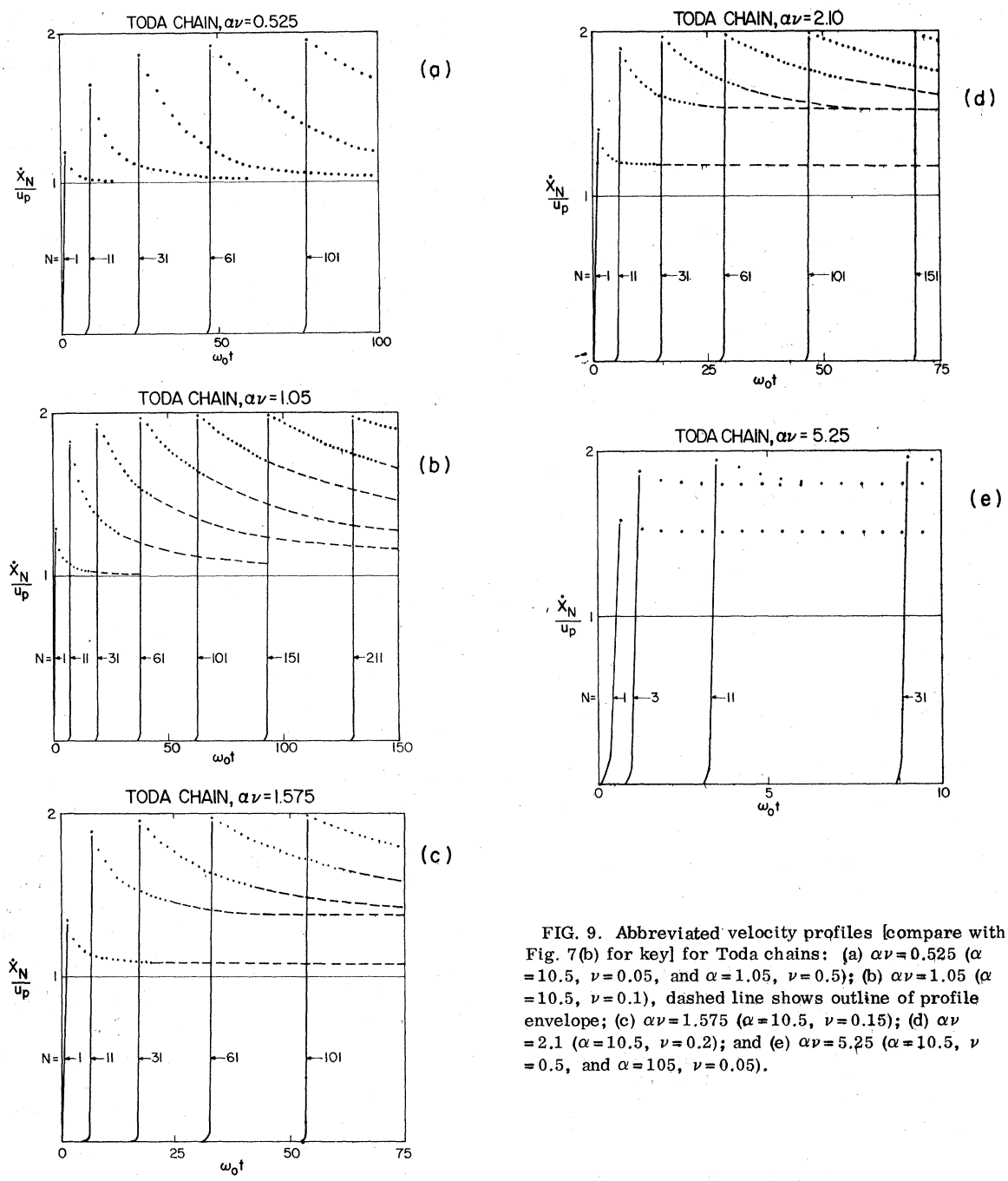

FIG. 9. Abbreviated velocity profiles [compare with Fig. 7(b) for key] for Toda chains: (a) $\alpha\nu = 0.525$ ($\alpha = 10.5$, $\nu = 0.05$, and $\alpha = 1.05$, $\nu = 0.5$); (b) $\alpha\nu = 1.05$ ($\alpha = 10.5$, $\nu = 0.1$), dashed line shows outline of profile envelope; (c) $\alpha\nu = 1.575$ ($\alpha = 10.5$, $\nu = 0.15$); (d) $\alpha\nu = 2.1$ ($\alpha = 10.5$, $\nu = 0.2$); and (e) $\alpha\nu = 5.25$ ($\alpha = 10.5$, $\nu = 0.5$, and $\alpha = 105$, $\nu = 0.05$).

locity profiles, and therefore, the shock velocity also, depend only on the product $\alpha\nu$, the shock strength parameter, as has been reported previously for weak shocks ($0.1 \leq \alpha\nu \leq 1$) in chains of particles interacting via the cubic potential.[4] We have found that this scaling of the shock strength applies over a much wider range of shock strengths and potential forms, namely, $0.105 \leq \alpha\nu \leq 52.5$ for the Toda potential along with selected comparisons with the LJ 6-12 and Morse potentials. Abbreviated velocity profiles are presented in Figs. 9(a)–9(e) with a full velocity profile for the strongest shock shown in Fig. 10. Data on shock velocity μ as a function of α, β, and ν for the various computer experiments are given in Table II and μ vs $\alpha\nu$ in Fig. 11.

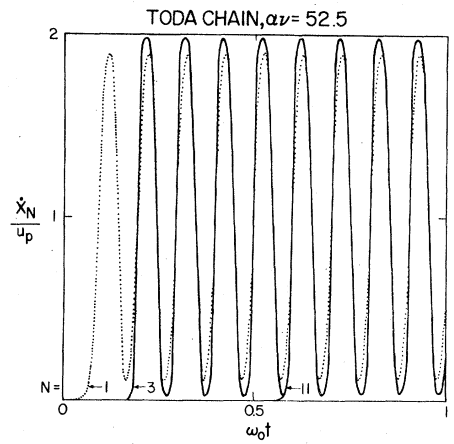

FIG. 10. Velocity profiles (full) for the strongest shock studied in the Toda chain, $\alpha\nu = 52.5$ ($\alpha = 10.5$, $\nu = 5$, and $\alpha = 105$, $\nu = 0.5$).

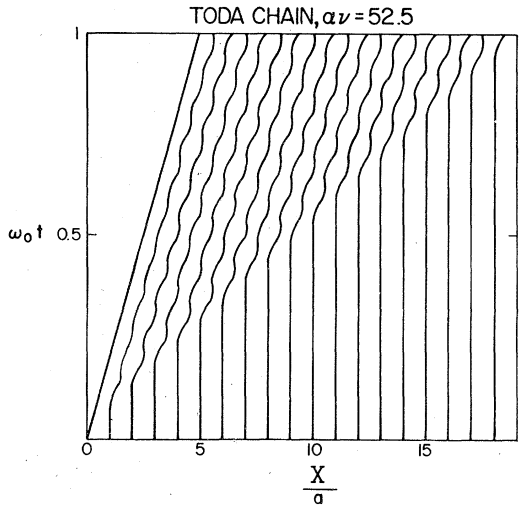

FIG. 12. Shock-wave trajectories of particles in a one-dimensional Toda chain, $\alpha\nu = 52.5$ ($\alpha = 10.5$, $\nu = 5$). See Fig. 3 for comparison with hard-rod chain and key.

Examination of Figs. 9(a)–9(e) reveals a surprising transition in the long-time behavior of the velocity profiles. At values of shock strength $\alpha\nu$ less than about one, the profiles converge to the particle velocity, while at larger values of $\alpha\nu$, the profiles reach a steady oscillatory state about the particle velocity. By the time $\alpha\nu = 52.5$, the solutions look very much like the hard-rod case, as comparison of Figs. 3 and 12 and of Figs. 4 and 13 shows. The steady profiles thus indicate that for sufficient shock strength in anharmonic chains—just as in the hard-rod case—an initial zero temperature in the unshocked region gives way to a finite final temperature after the shock wave passes. A measure of the ratio of the internal kinetic energy to the center-of-mass kinetic energy behind the shock is given by

$$\epsilon = \lim_{t\to\infty}[\max(\dot{x}_N(t)/u_p - 1)^2], \tag{38}$$

which is plotted against $\alpha\nu$ in Fig. 14. In the harmonic limit ($\alpha\nu \to 0$), $\epsilon \to 0$; while in the anharmonic hard-rod limit ($\alpha\nu \to \infty$), $\epsilon \to 1$; hence, ϵ exhibits the transition to hard-rod behavior at $\alpha\nu \gtrsim 1$. As

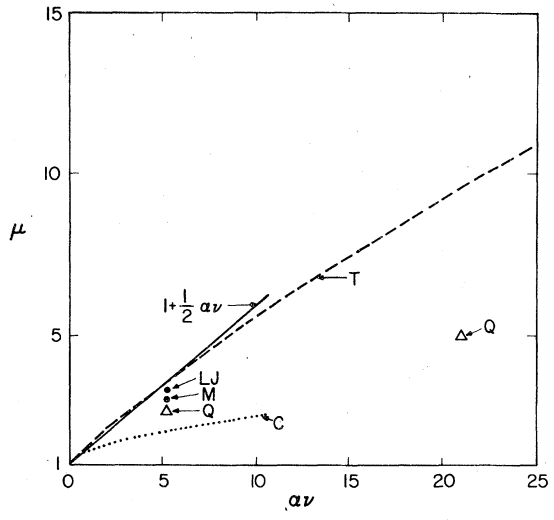

FIG. 11. Shock velocity $\mu = u_s/c_0$ as a function of shock strength $\alpha\nu(\nu = u_p/c_0$ and α is the cubic anharmonicity). $\mu = 1 + \frac{1}{2}\alpha\nu$ is the linear result for the continuum approximation to shock-wave propagation [Eqs. (40) and (41)]. *C*, cubic chain; *Q*, quartic; *T*, Toda; LJ, LJ 6-12; *M*, Morse.

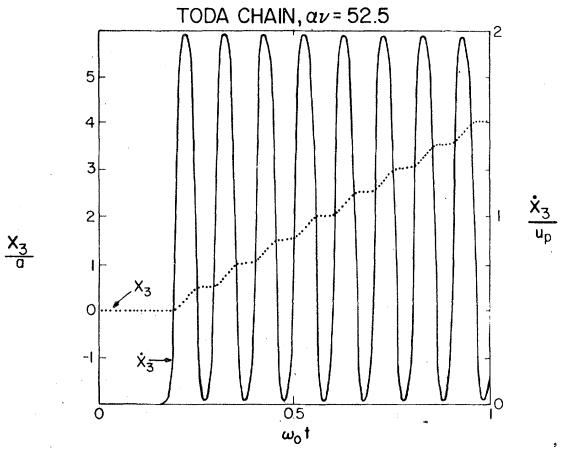

FIG. 13. Velocity response $\dot{x}_3$ (solid line) of Toda particle number three to a shock wave as a function of time; its displacement x_3 from its lattice site $X_3(0) = 3a$ is also shown (dotted line). For comparison with hard-rod chain, see Fig. 4.

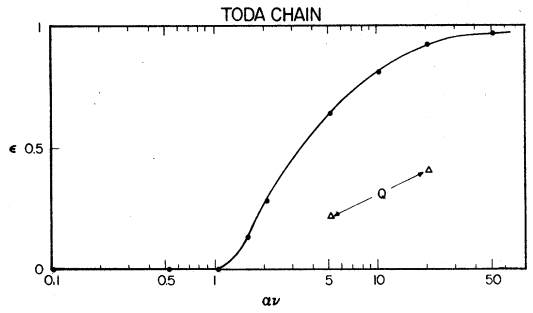

FIG. 14. The thermal parameter ϵ [Eq. (38)] as a function of shock strength αv for Toda chains; quartic chains shown as Q.

shock strength αv is increased, the relaxation time from the initial velocity response to the final steady state divided by particle number, τ_N/N, also increases, though more slowly in the regime where $\alpha v \gtrsim 1$.

The full potentials (Toda, LJ 6-12, Morse) and the quartic truncated potential exhibit the approach to hard-rod behavior—steady velocity profiles—with increasing shock strength, while the cubic truncated potential does not, even up to the point where the potential barrier to interpenetration of particles, which depends on α, is close to the maximum relative kinetic energy, $\frac{1}{2}(2v)^2 = 2v^2$. The cubic chain has profiles that continue to look qualitatively like Fig. 9(a). The quartic chain exhibits hard-rod-like steady profiles more slowly as a function of shock strength than the full potentials; for example, at $\alpha v = 21$, $\epsilon = 0.4$, while the Toda potential gives $\epsilon = 0.4$ at $\alpha v \cong 2.7$ (see Fig. 14). The failure of the cubic chain to show hard-rod behavior is undoubtedly due to the anomalous repulsive force at larger separations than the equilibrium value (see Fig. 2).

Tasi[7] has concluded from a far-field analysis of weak shocks in a cubic chain ($\alpha = 0.2$, $v = 0.1$, $\alpha v = 0.02$) that by $N = 1999$ the beginnings of a solitary-wave structure is observable in the velocity profile, that is, the second peak has begun to look like the first. By $N = 3999$, the first two peaks look identical, and by $N = 5999$, the first three look identical. Our molecular-dynamics calculations show no such solitary-wave behavior for this system. Indeed, our results for $N = 999$ agree with Tasi's numerical results (within the linewidth of his graph), though for integrating the equations of motion he used Hamming's modified predictor-corrector method rather than the central difference scheme outlined here. Had he integrated further, he would have found, as we did, that the far-field analysis becomes progressively worse with distance into the chain. In Fig. 15(a) is shown the molecular dynamics results as well as Tasi's far-field analysis for $N = 1999$. Note that the decay in the peaks of the molecular-dynamics velocity profile is concave upward (like an exponential decay) compared to concave downward for the far-field model. The disagreement is even more noticeable by $N = 3999$ in Fig. 15(b). The relaxation time calculated from the molecular-dynamics data is $t_N \cong 0.024N$ for $N = 999$, 1999, and 3999. One is forced to conclude that the solitary-wave behavior demonstrated by the far-field analysis for weak shocks in one-dimensional chains is due to some artifact not present in the full solution of the equations of motion.

Extending previous work on the continuum approximation to the equations of motion [Eq. (10)] for shocks in the cubic chain[4] to the quartic chain, we have the following results for the shock velocity:

$$\mu^2 = 1 + \alpha v/\mu + \beta v^2/\mu^2, \tag{39}$$

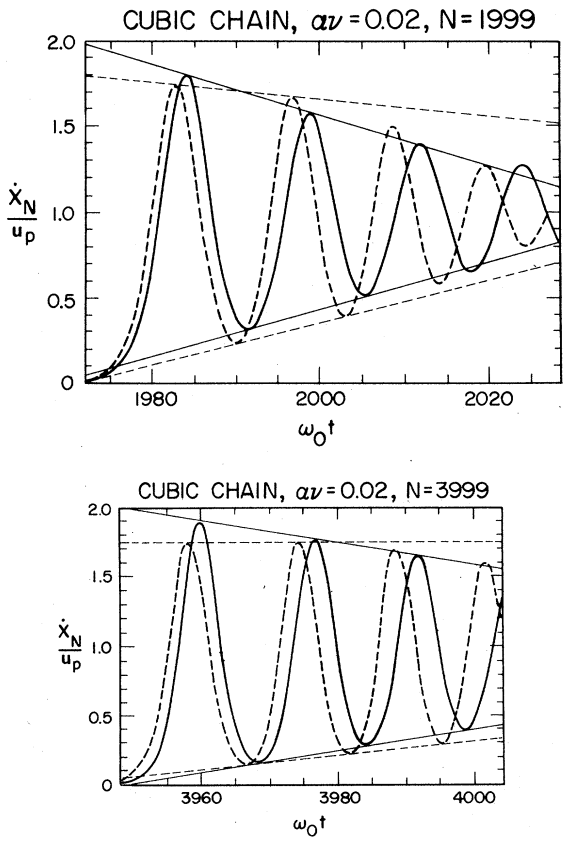

FIG. 15. Comparison of velocity profiles of molecular dynamics calculations (straight line) and Tasi's far-field perturbation analysis (short dashes) for a weak shock in a cubic chain ($\alpha = 0.2$, $v = 0.1$, $\alpha v = 0.02$). Straight lines have been drawn through the first two peaks and first two troughs to emphasize the differences in the decay envelopes of the exact result and the far-field analysis.

whence, after some algebraic manipulation,

$$\mu = 1 + \tfrac{1}{2}\alpha v - \tfrac{3}{8}(1 - \tfrac{4}{3}\beta/\alpha^2)(\alpha v)^2 + \cdots . \quad (40)$$

Since $\beta/\alpha^2 < \frac{3}{4}$ for the full potentials, μ curves down away from the linear result

$$\mu = 1 + sv , \quad (41)$$

where $s = \frac{1}{2}\alpha$, shown in Fig. 11. That this linear expression fits the Toda results moderately well up to $\alpha v \sim 8$ is fortuitous, since the continuum analysis breaks down for the quartic case [Eq. (40), $\beta/\alpha^2 = \frac{2}{3}$] at about this point and is therefore not really very useful.

The full potentials give velocity profiles that differ only slightly from each other. The small differences in shock velocity can be approximately corrected by linear interpolation in β/α^2. The shock velocities for the cubic, Morse, LJ 6-12, and Toda potentials can be fit approximately by the following empirical form, given the Toda chain shock velocity $\mu(\alpha v, \frac{2}{3})$:

$$\mu(\alpha v, \beta/\alpha^2) \cong \mu(\alpha v, \tfrac{2}{3}) + 0.459\alpha v \times [1 - \exp(-1.089\alpha v)](\beta/\alpha^2 - \tfrac{2}{3}). \quad (42)$$

The Toda chain shock velocity for $\alpha v \lesssim 5$ is given approximately by

$$\mu(\alpha v, \tfrac{2}{3}) = 1 + 0.633\alpha v - 0.0314(\alpha v)^2 . \quad (43)$$

For the Toda chain, we have studied the limit of the initial frequency of the velocity response far from the piston given by [see Eq. (32)]

$$\omega_1 = \lim_{N\to\infty} 2\pi/t_N^{(1,3)} , \quad (44)$$

and the final (long-time) frequency, which is given by

$$\omega_\infty = \lim_{N\to\infty} \lim_{n\to\infty} 2\pi/t_N^{(2n-1,2n+1)} . \quad (45)$$

In the harmonic limit $\omega_1 = 0$ and $\omega_\infty = 2\omega_0$, the maximum frequency in the harmonic-chain spectrum. In the hard-rod limit, $\omega_1 = \omega_\infty = 2\pi/t_c$. In Fig. 16, ω_1 and ω_∞ are shown as functions of shock strength αv for the Toda chain.

In the harmonic chain, the initial frequency of the velocity profile for particle N is low, on the order of $\omega_0/N^{1/3}$ [see Eq. (32)], and slowly increases to $2\omega_0$, in essence sampling the entire frequency range of the harmonic spectrum. After some distance into the anharmonic chain, however, the initial frequency no longer decreases, but reaches some small limiting value. The particle then oscillates faster and faster with time, reaching a higher value than the $2\omega_0$ of the harmonic chain. For stronger and stronger shocks, both of these frequencies increase, but the range of frequencies narrows until the hard-rod limit is reached, where there is only one frequency in the system—the hard-rod collision frequency. From Fig. 16, it appears that $\omega_1 \to \omega_\infty \to \alpha v$. From Eq. (20), we see that the hard-rod collision frequency is also linear in the particle velocity.

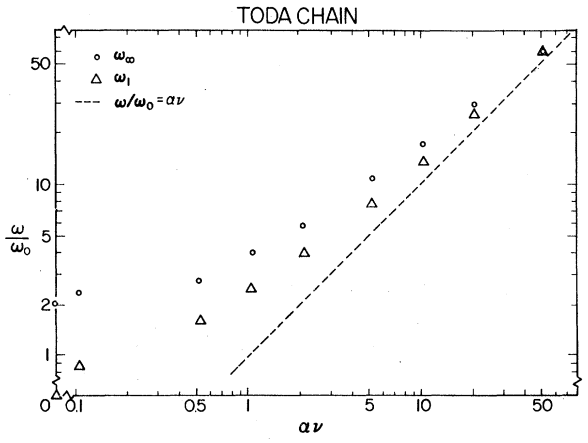

FIG. 16. Initial oscillatory frequency of velocity response ω_1 for particles far from the piston (asymptotic) and the final long-time value (after the initial rise) ω_∞ as a function of shock strength αv in Toda chains. Dashed line is the function αv. Note the break in the logarithmic scale near the origin so as to show the harmonic-chain limits.

VII. EFFECTS OF TEMPERATURE AND OF MASS DEFECTS

When we observed that particle velocity profiles for weak shocks in anharmonic chains evolved with distance toward hard-rod-like steady profiles, we were naturally led to wonder whether disruption of perfect lattice symmetry ahead of the shock wave would prevent the growth of hard-rod-like waves. To that end we equilibrated a Morse chain at a finite temperature, $k_B T/mc_0^2 \cong 10^{-5}$, which is a few degrees Kelvin for a typical metal, and then sent a weak shock down the chain ($\alpha = 10.5$, $v = 0.05$, $\alpha v = 0.525$). The results for two particles far down the chain from the piston are shown in Fig. 17. We see that the random thermal fluctuations ahead of the shock are swamped by the highly correlated, almost steady waves that have evolved. Essentially no effect on the shock-wave propagation is discernible save the modulations due to superimposed thermal fluctuations; for example, the tiny apparent increase in shock velocity is hardly bigger than the experimental error ($\lesssim 1\%$). An order of magnitude higher initial temperature naturally makes the

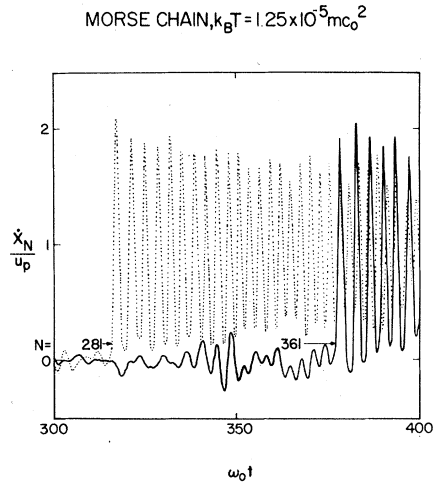

FIG. 17. Two velocity profiles of particles in an initially thermalized Morse chain, $k_BT/mc_0^2 \cong 10^{-5}$, $\alpha v = 0.525$ ($\alpha = 10.5$, $v = 0.05$).

signal harder to pick out from the noise, but the same relentless growth of anharmonic response is ultimately observed. When an order of magnitude stronger shock is sent through a Morse chain at this higher temperature, the hard-rod-like steady profiles are basically unchanged, since both the magnitude of the thermal fluctuations and their frequency are much smaller than those of the steady-velocity waves behind the shock. If the random fluctuations are subtracted out both before and after the shock front has passed, the only temperature rise we observe is due to the steady-wave (hard-rod-like) response for strong shocks.

We have discussed the mechanisms of thermal relaxation by analogy with the limiting models of collisional transfer of thermal energy afforded by the harmonic and hard-rod chains. A critical question which may be impossible to resolve is: After a shock wave has passed a point in the hard-rod chain, does the shocked portion *never* reach equilibrium, or is it already instantaneously in

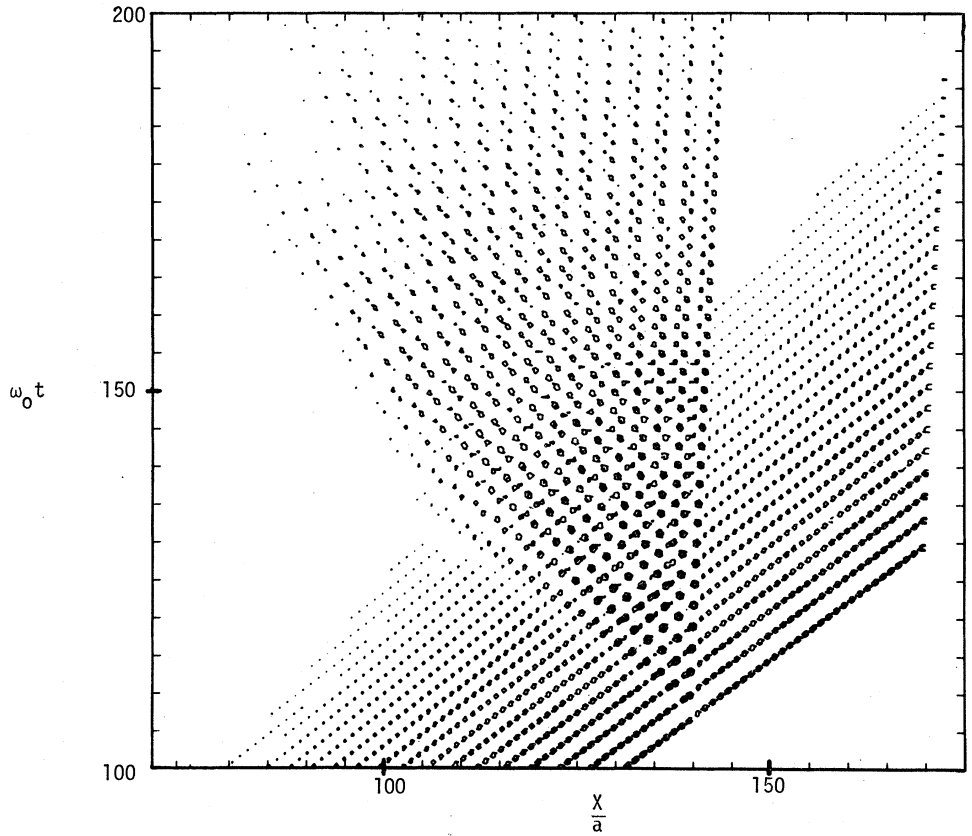

FIG. 18. Velocity contour plot vs position and time (see Fig. 6) for a shock wave hitting a mass defect in a Toda chain, $m_{139}/m = 1.5$, $\alpha v = 0.525$ ($\alpha = 10.5$, $v = 0.05$). Contours are drawn at $1.35\,u_p$ ($1/e$-fold decay from $2u_p$ to u_p) and $1.7\,u_p$.

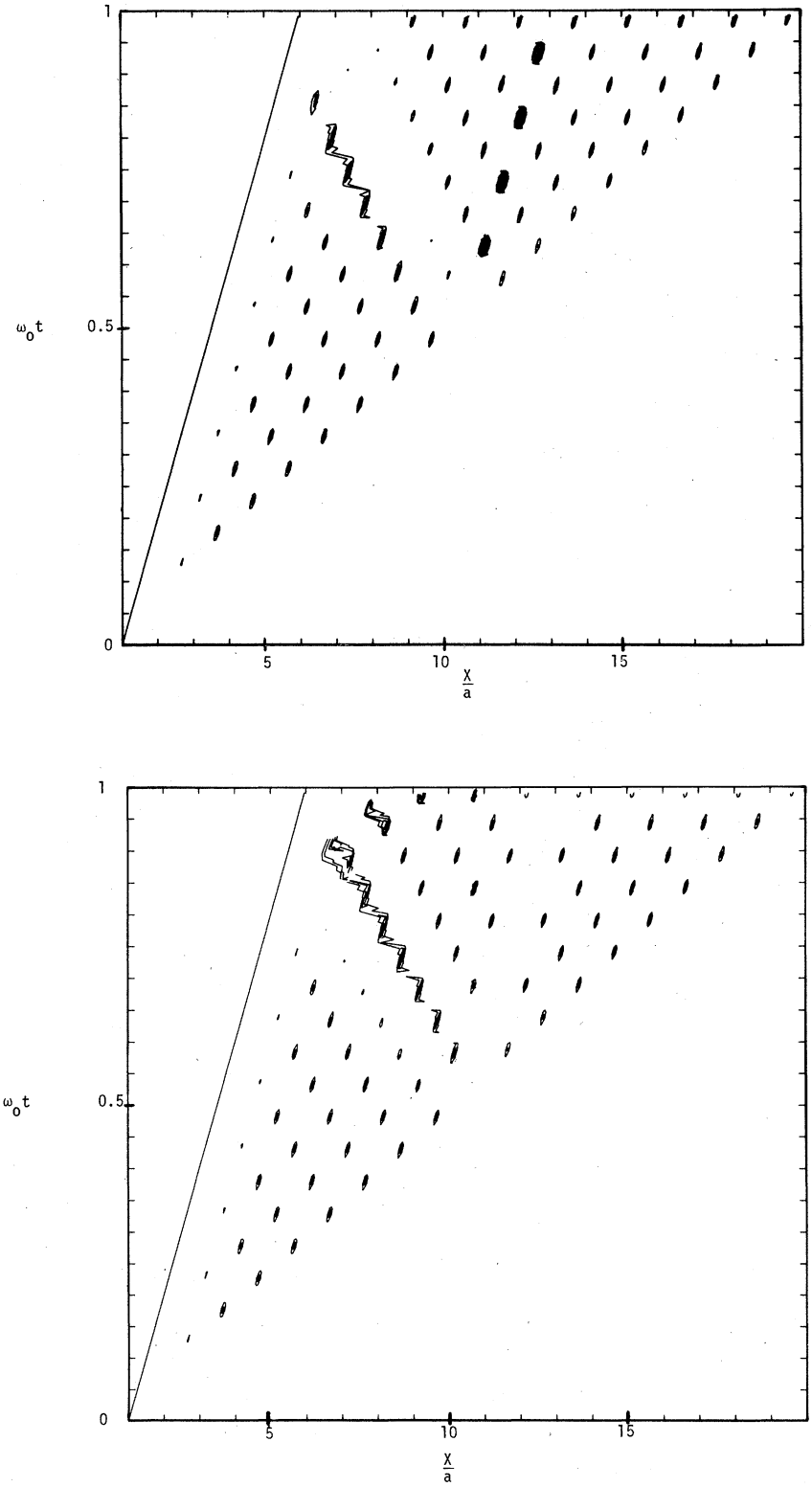

FIG. 19. Velocity contour plots vs position and time (see Fig. 6 for comparison with the hard-rod chain) for a mass defect at particle number 9 in a Toda chain, $\alpha v = 52.5$ ($\alpha = 10.5$, $v = 5$): (a) $m_9/m = 0.8$, contours at 1.85, 1.95, 2.05, and 2.15 u_p; (b) $m_9/m = 1.2$, contours at 1.8, 1.9, and 2.0 u_p.

equilibrium? It certainly never reaches the state of *random* fluctuations that we usually associate with a finite temperature, even though we can easily calculate a final temperature from a standard statistical-mechanical formula

$$k_B T = \lim_{t\to\infty} \frac{1}{t} \int_{t_s}^{t_s+t} dt' \, \frac{1}{N} \sum_{i=1}^{N} m[\dot{x}_i(t') - u_p]^2 , \quad (46)$$

where k_B is the Boltzmann constant and N is a collection of particles which have been shocked by the time $t = t_s$.

We have also investigated the effect of mass defects, both lighter and heavier than the other members of the chain, to determine whether the presence of such defects can speed up the relaxation process behind the shock front, as is often supposed. The following Toda chains, with mass defects far enough down the chain that the initial velocity response has reached its asymptotic value, have been studied: $\alpha v = 0.525$ and 5.25, $m = 0.5$, 0.8, 1.2, and 1.5; and $\alpha v = 52.5$, $m = 0.8$ and 1.2. As an example the velocity-contour plot versus position and time, with contours drawn near the $1/e$-fold value, $1.35u_p$, and at $1.7u_p$, is presented in Fig. 18 for $\alpha v = 0.525$, $m = 1.5$. Compare this with Fig. 6 for hard rods. The disturbances due to the heavy-mass defect ($N = 139$) are very apparent. Though the fine details differ, qualitatively very similar results are obtained for a light defect, that is, the energy of the shock wave is partially backscattered by any mass defect. Quantitative agreement with the hard-rod problem in Sec. IV, including details of individual collisions, is approached in the essentially hard-rod $\alpha v = 52.5$ cases. For example, the reflection velocity calculated according to Eq. (23) is $V_r/c_0 = -12.5$ ($\mu = 19.7$, $-\mu/\eta = -14.7$) for $\delta = -0.2$, while $V_r/c_0 = -13.1$ is observed. For $\delta = +0.2$, $V_r/c_0 = -16.5$ is calculated, while $V_r/c_0 = -16.0$ is observed. The shock velocity following the defect is predictably [see Eq. (24)] only slightly slowed by the defect (~1%), which is difficult to detect. In Figs. 19(a) and 19(b), contour plots of these very anharmonic problems are presented for comparison with the hard-rod case in Fig. 6.

The mass defects do not lead to a quickening of the relaxation to equilibrium behind the shock front. On the contrary, behind the defect the relaxation process is noticeably slowed down because of interference from waves backscattered off the defect. Beyond the defect, as is clearly visible in Fig. 18, the relaxation process resumes almost as if no defect were there, that is, a straight-line relaxation rear can be drawn. Thus, in addition to the constant fraction of unequilibrated material behind the shock characteristic of anharmonic chains are these regions of backscattered disturbance due to the presence of mass defects.

It is easy to speculate on the effect of mass defects in three-dimensional crystals. Very likely they cause scattering and smearing of the shock waves; however, the presence of extended defects and the possibility of plastic flow in higher dimensions make it rather risky to draw incisive conclusions from our one-dimensional results. We are therefore pursuing these questions in three-dimensional molecular-dynamics calculations.

ACKNOWLEDGMENTS

We would like to thank Duane Wallace for stimulating discussions that have helped clarify the goals of our research on shock-wave structure. This work was supported in part by the U.S. Department of Energy.

[1] D. H. Tsai and C. W. Beckett, J. Geophys. Res. 71, 2601 (1966).
[2] R. Manvi, G. E. Duvall, and S. C. Lowell, Int. J. Mech. Sci. 11, 1 (1969).
[3] D. H. Tsai and C. W. Beckett, "Shock Wave Propagation in a Two-Dimensional Crystalline Lattice," in *Behavior of Dense Media Under High Dynamic Pressure*, Paris, 1967 (Gordon and Breach, New York, 1968), pp. 99–108.
[4] G. E. Duvall, R. Manvi, and S. C. Lowell, J. Appl. Phys. 40, 3771 (1969).
[5] R. Manvi and G. E. Duvall, J. Phys. D 2, 1389 (1969).
[6] J. Tasi, J. Appl. Phys. 43, 4016 (1972).
[7] J. Tasi, J. Appl. Phys. 44, 4569 (1973).
[8] D. H. Tsai and R. A. MacDonald, J. Phys. C 6, L171 (1973).
[9] D. C. Wallace (private communication).
[10] J. O. Hirschfelder, C. F. Curtiss, and R. B. Bird, *Molecular Theory of Gases and Liquids* (Wiley, New York, 1954), p. 783 ff.
[11] B. J. Alder and T. E. Wainwright, J. Chem. Phys. 31, 459 (1959).
[12] J. B. Gibson, A. N. Goland, M. Milgram, and G. H. Vineyard, Phys. Rev. 120, 1229 (1960).
[13] W. T. Ashurst and W. G. Hoover, Phys. Rev. A 11, 658 (1975).
[14] M. Toda, J. Phys. Soc. Jpn. 22, 431 (1967).
[15] *Handbook of Mathematical Functions*, edited by M. Abramowitz and I. A. Stegun (National Bureau of Standards, Washington, D. C., 1967), p. 358 ff.
[16] G. Leibfried, "Gittertheorie der mechanischen und thermischen Eigenschaften der Kristalle," in *Handbuch der Physik*, edited by S. Flügge (Springer-Verlag, Berlin, 1955), Vol. VII, pp. 104–324.
[17] We have also generated shock waves in a periodic chain of N particles by continually reducing the length

according to $L(t) = Na - 2u_p t$. A right-running shock wave proceeds from the left boundary while a left-running shock wave proceeds from the right boundary. Until they collide, the results are the same as for the the piston-particle boundary condition, except that the initial particle velocity response reaches its asymptotic value nearer to the boundary in the shrinking periodic scheme.